Cardiovascular Research, 1973, **7**, 105–114.

Mathematical model of A-V conduction in the rat heart

ROBERT M. HEETHAAR, JAN. J. DENIER VAN DER GON, and FRITS L. MEIJLER
From the Department of Medical Physics, University of Utrecht and from the Department of Cardiology, University Hospital, Utrecht, The Netherlands

AUTHORS' SYNOPSIS To study A-V nodal conduction of the rat heart the right atrial appendage was stimulated with a variety of pulse sequences. The response was detected with ventricular epicardial electrodes. From the observed relations between P–P and P–R intervals a mathematical model describing A-V nodal conduction has been derived. The model was tested by random atrial stimulation and proved to describe A-V nodal conduction quantitatively.

Ventricular dysrhythmia associated with atrial fibrillation has been ascribed to concealed conduction within the A-V node (Moe and Abildskov, 1964; Moore, 1967). The slowing of the ventricular rhythm in patients with atrial fibrillation in response to digitalis has been attributed to alteration in A-V nodal behaviour (Horan and Kistler, 1961). However, the intrinsic conductive properties of the A-V node as well as the role of the atria (Bootsma, Hoelen, Strackee, and Meijler, 1970) are not sufficiently understood to explain these phenomena quantitatively (Brody, 1970).

This paper presents a quantitative analysis of A-V nodal conduction in the rat heart as an attempt at a better understanding of the A-V nodal conductive mechanism. Since the A-V node is not easily accessible to direct observation without changing its function, electrical impulses were applied to the atrium and the resulting ventricular responses were detected. Next, relations between the stimulating intervals (P–P intervals) and the stimulus-response times (P–R intervals) were analysed. From these relations, observed during fixed atrial stimulation rates and step changes in stimulation frequency, a mathematical model describing A-V nodal conduction has been derived.

As a check on the model the heart was stimulated randomly to see if the model could accurately predict A-V nodal behaviour.

Methods

1. Isolated perfused hearts

White rats, weighing 200 to 300 g, were anaesthetized with ether. The hearts were rapidly removed and perfused according to Langendorf with a modified Tyrode solution (Meijler, Offerijns, Willebrands, and Groen, 1959), in equilibrium tensions with a mixture of O_2 (95%) and CO_2 (5%). The temperature was controlled at $36{\cdot}0° \pm 0{\cdot}2°C$. Platinum bipolar stimulating electrodes were stitched to the right atrial appendage. The left ventricular electrogram was detected with the same type of bipolar epicardial electrodes. The heart was stimulated with rectangular pulses from a triggered current source (Goovaerts, Schneider, and Zimmerman, 1971), having a pulse-width of 1·0 msec and a strength of twice the threshold (usually ≈ 1 mA). It was possible to stimulate with several pulse sequences such as fixed rates and steps in frequency. Random rhythms could be generated by a radioactive source which triggered an electronic device with an adjustable dead-time, to prevent blocking of atrial activation in the A-V node and with an adjustable maximum interval to prevent spontaneous nodal or ventricular pacemaker activity. The

stimulus artefacts and the amplified ventricular responses were recorded on magnetic tape. The low frequency components (<2 Hz) of the electrogram were filtered out to increase baseline stability. All measurements were achieved within 1 hr. To measure simultaneously P–P and P–R intervals (defined below in 'Analysis') two H.P. 5325 B counters were used. By means of a teletype connected to the BCD output channels of the counters the P–P and P–R intervals were transmitted to papertape which could be used as input to a PDP 15/40 computer.

2. Hearts *in situ*

Rats were anaesthetized with ether. While artificial respiration was applied, the heart was exposed by a midsternal thoracotomy. Bipolar stimulating and recording electrodes were stitched to the right atrial appendage and left ventricle in the same way as in the isolated heart (see above). The recording and stimulating techniques described above were used.

3. Analysis

The intervals between stimulating pulses are considered here as the input signals of the A-V node (P–P intervals). This is allowable since, irrespective of stimulating rate, the changes in time between stimulus artefact and atrial activation were negligible (see also Results section). The intervals between the stimulating pulses and the corresponding R waves are considered as the output of the system (P–R intervals).

This P–R interval consists of three components: (1) pulse propagation time from stimulating electrodes over the atrial myocardium to the A-V node; (2) transmission time through the A-V node; (3) conduction time from the A-V node to the left ventricular epicardial electrodes.

As the time required for impulse propagation over the atria and ventricles is almost constant and much less than the conduction time in the A-V node, the measured delay between stimulating pulse and ventricular response occurs mainly in the A-V node. The contribution of the impulse propagation over the atria and ventricles on the resulting P–R interval is dealt with in detail in the Results section.

Results

1. Fixed rates

When the atrium of the isolated heart is stimulated at a fixed rate the P–R interval is constant within 0·2 msec. Decrease of the stimulating interval gives an increase in A-V conduction time and vice versa. Figure 1 shows a plot of the P–R intervals as a function of steady state P–P intervals in a typical experiment. The plot is limited on the left side because a further decrease of the P–P interval would cause blocking of atrial activations in the A-V node. On the right side it is limited because of the escape mechanism or the spontaneous rate of the S-A node.

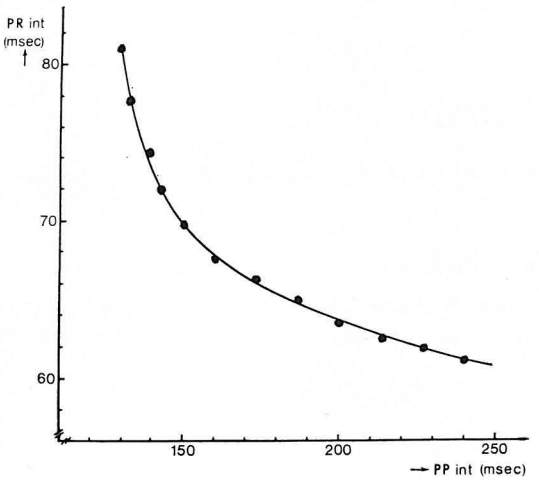

FIG. 1 *Steady state relation between P–R and P–P intervals.*

2. Frequency steps

As second input signal, a step in frequency has been used – that is, a regular rhythm is changed at a given instant to another regular rhythm. The typical changes in P–R intervals after such steps are shown in Fig. 2. From all experiments it appears that adaptation of the A-V node to the new stimulating interval is achieved within four to eight beats after the change of the P–P interval. It can be seen that adaptation to long intervals takes fewer beats than adaptation to short intervals. The number of beats is found to be less important than the time in which the transition occurs. In Fig. 3 the response to one step is shown. The A-V nodal conduction time (P–R interval) in the first steady state with a P–P interval τ_0 is given by g_0, the P–R interval after adaptation to the second steady state with stimulating interval τ_1 by g_∞, and the P–R

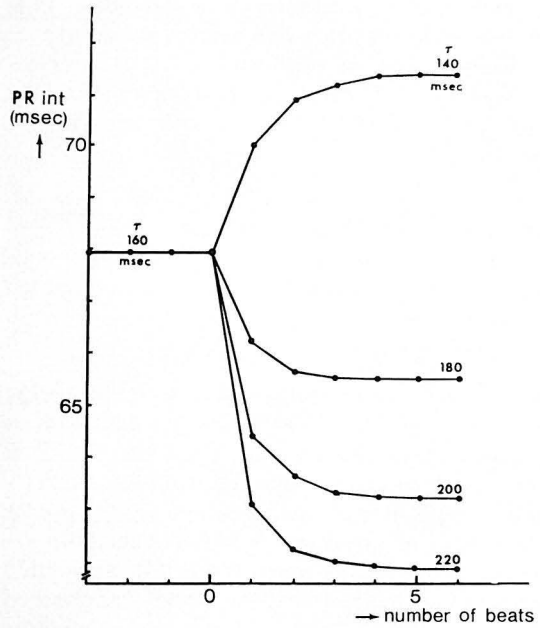

FIG. 2 *Course of P–R interval after steps in stimulating interval from 160 to 140, resp. 180, 200, and 220 msec.*

interval after the i-th stimulating pulse after the frequency step by g_i (i=1, 2, 3 . .). From all steps it appears that the P–R interval g_i after the frequency step can be described by a simple exponential relation:

$$g_i - g_\infty = (g_0 - g_\infty)e^{-\lambda t} \qquad (1)$$

where t is the time elapsed after the frequency was switched and $1/\lambda$ is a time constant. A semilogarithmic plot of $g_i - g_\infty$ as a function of t for different steps in frequency is shown in Fig. 4. The slopes of these curves give the value of λ. From these slopes it can be concluded that the time constant $1/\lambda$ is independent of the initial and final value of the step. The time constant of all the rat hearts studied was found to be in the same order of magnitude. However, this time constant turned out to depend strongly on the temperature of the heart.

Theoretical interlude

After a frequency step the P–R intervals (g_i) are given by relation (1). Substitution of $t = i\tau_1$ gives:

$$g_i - g_\infty = (g_0 - g_\infty)e^{-\lambda i\tau_1} \qquad (2)$$

This implies that:

$$g_{i+1} - g_\infty = (g_0 - g_\infty)e^{-\lambda i\tau_1}.e^{-\lambda\tau_1} \qquad (3)$$

Substitution of (2) in (3) gives:

$$g_{i+1} - g_\infty = (g_i - g_\infty)e^{-\lambda\tau_1}$$

This relation holds for steady states as well as for frequency steps. We now postulate (as a hypothesis) that this relationship should hold in general, which means that the A-V conduction time g_n at a certain moment is given by the expression:

$$g_n = g_{n,\infty} + (g_{n-1} - g_{n,\infty})e^{-\lambda\tau_n} \qquad (4)$$

where τ_n = the P–P interval preceding g_n.
$g_{n,\infty}$ = the P–R interval in case of a steady state with a stimulating interval τ_n.
g_{n-1} = the P–R interval preceding g_n.

In Fig. 5 impulse propagation of an irregular rhythm through the A-V node is shown schematically with the stimulating intervals τ_i and the corresponding P–R intervals g_i. Substitution of g_{n-1} for i=1, 2, 3, 4 (see Appendix) in (4) results in an expression for g_n only as a function of the five direct preceding intervals. The influence of other intervals preceding the last five can be omitted as is shown in the Appendix. The result is:

$$g_n = \rho(\tau_n) + \sum_{j=1}^{4} \rho(\tau_{n-j}) \exp\{-\lambda \sum_{i=0}^{j-1} \tau_{n-i}\} \qquad (5)$$

where $\rho(\tau_n) = g_{n,\infty}(1 - e^{-\lambda\tau_n})$

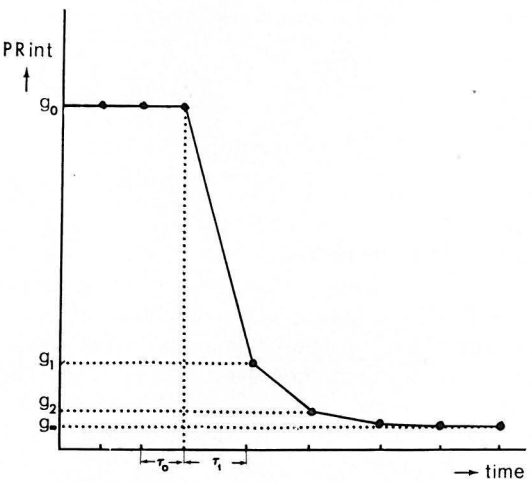

FIG. 3 *Course of P–R interval after a step in stimulating interval from τ_0 to τ_1 msec illustrating symbols used in the text.*

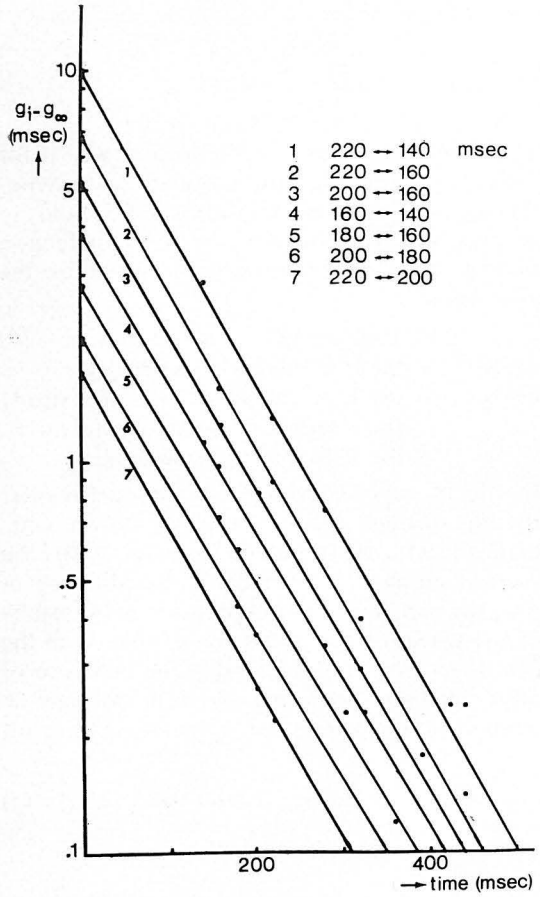

FIG. 4 *Semi logarithmic plot of $g_t - g_\infty$ as a function of the time t after different steps in stimulating interval.*

For abbreviation this relation is noted as:

$$g_n = F(\tau_n, \tau_{n-1}, \ldots, \tau_{n-4}) \qquad (6)$$

3. Random stimulation

The hypothesis mentioned above has been tested by random stimulation of the rat heart, subject to the condition that the P–P intervals are within the range of the applied fixed interval rates. The results are shown in Fig. 6. This Figure shows a plot of the measured P–R intervals together with the computed results of 50 successive beats during a random rhythm. The correspondence between the curves is fair and within the experimental error. The influence of each of the several preceding P–P intervals on a predicted P–R interval from 50 successive beats is shown in Fig. 7. Figure 7A plots the measured P–R intervals versus the P–R intervals, computed from the last preceding P–P interval with help of the formula:

$$g_n = F(\tau_n, \tau_0, \tau_0, \ldots, \tau_0)$$

where τ_0 is the mean P–P interval.

Figure 7B shows calculated P–R intervals versus the measured P–R intervals, computed from two preceding intervals:

$$g_n = F(\tau_n, \tau_{n-1}, \tau_0, \tau_0, \tau_0)$$

In Fig. 7C also the influence of three preceding P–P intervals for P–R interval calculation is demonstrated. Finally, in Fig. 7D the P–R intervals have been computed from four directly preceding P–P intervals. It can be seen that now the spread of the points is almost negligible.

The above results were obtained from isolated perfused rat hearts. Next the model was checked on rat hearts *in situ* by carrying out the same experiments. After the end of such an experiment, which lasted about 1 hr, the heart was rapidly removed from the body and connected to the perfusion apparatus. Again the same measurements were carried out.

From the results obtained, it appears that the same relationships hold for the heart *in situ* as well as for the isolated perfused heart. The time constant $1/\lambda$ which is a measure for the adaptation to the A-V node to changes in frequency is in the same order of magnitude (for the heart *in situ*: 120 msec, $T \simeq 36°C$; for the isolated perfused heart: 110 msec, $T = 36{\cdot}0°C$). In case of the heart *in situ* for obvious reasons the temperature could not be controlled as accurately as during perfusion.

Figure 8 shows a plot of the P–R intervals computed from the P–P intervals during random stimulation of the heart *in situ*. Again there is an acceptable correspondence between the experimental and computed results.

4. Calculation of P–P and P–R intervals from measured R–R intervals

With the model it is also possible to derive P–P and P–R intervals from measured R–R intervals during random stimulation when the time constant $1/\lambda$ and the steady state relation

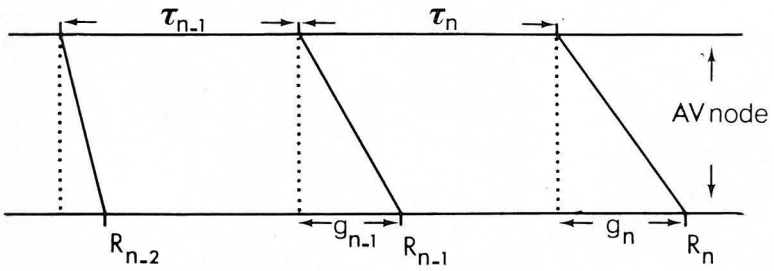

FIG. 5 *Schematic representation of the pulse propagation through the A-V node illustrating symbols used in the test.*

$g_\infty = g_\infty(\tau)$ are known. From Fig. 5 it can easily be seen that the R–R interval between the two R waves R_n and R_{n-1} is given by the expression:

$$RR_n = \tau_n + g_n - g_{n-1} \qquad (9)$$

As g_n is a function of τ_{n-1} (i=0, 1, . . ., 4) the equation becomes:

$$RR_n = \tau_n + g(\tau_n, \ldots, \tau_{n-4}) - g(\tau_{n-1}, \ldots, \tau_{n-5})$$

When a sequence of R–R intervals during random stimulation is measured the corresponding P–P intervals can be calculated as is done below. The first P–P interval τ_1 is calculated with the help of the computer so that the relation holds:

$$RR_1 = \tau_1 + g(\tau_1, \tau_0, \tau_0, \tau_0, \tau_0) - g(\tau_0, \tau_0, \tau_0, \tau_0, \tau_0)$$

where τ_0 is an arbitrary P–P interval.

With this interval τ_1 the next P–P interval τ_2 is calculated so that:

$$RR_2 = \tau_2 + g(\tau_2, \tau_1, \tau_0, \tau_0, \tau_0) - g(\tau_1, \tau_0, \tau_0, \tau_0, \tau_0)$$

Repeated calculations give the results shown in Fig. 9. In this Figure the measured P–R and P–P intervals are shown together with those computed from measured R–R intervals during

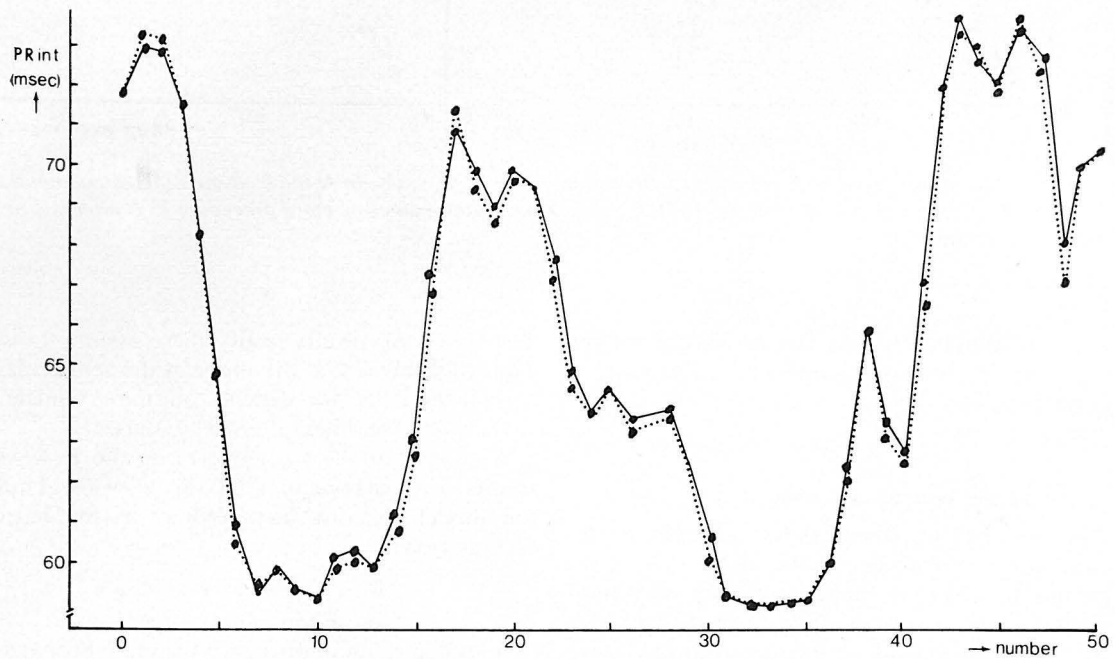

FIG. 6 *Representation of fifty successive measured P–R intervals* (continuous line) *and the computations of the model* (dashed line) *during random stimulation of the isolated rat heart.*

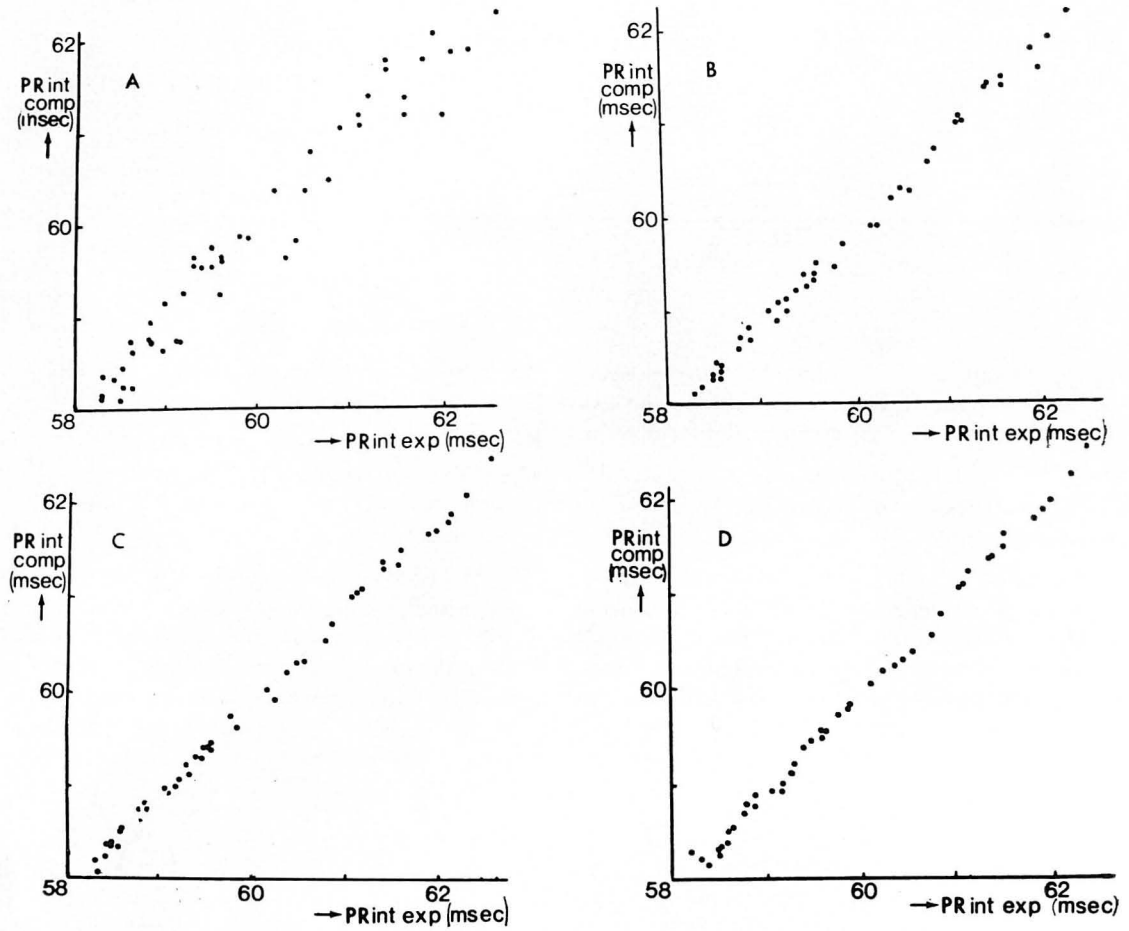

FIG. 7 *Plot of measured P–R intervals versus computed P–R intervals. In* A *the P–R intervals are computed from the direct preceding P–P interval. In* B, C, *and* D *the actual values of more preceding P–P intervals are taken into account.*

random stimulation. The fast convergence after five to six beats shows that there is an acceptable correspondence between theoretical and experimental results.

5. Atrial and ventricular conduction

The method described above to analyse the conductive properties of the A-V node from atrium to ventricle makes use only of input–output relations without looking inside the node. In the experimental set-up assumptions were made concerning impulse propagation over the atrial and ventricular myocardium (see analysis). The following results justify these assumptions. Figure 10 shows that the shape of the ventricular complexes does not depend on the frequency within the experimental error (0·3 msec).

A change of the trigger level on the R wave results in a change of all P–R intervals. Thus the model remains unaltered as in the basic formulation:

$$g_n - g_{n,\infty} = (g_{n-1} - g_{n,\infty})e^{-\lambda\tau_n}$$

only differences of conduction times appear.

A second point of interest is the pulse propagation over the atria. In Fig. 11 P waves are shown at various stimulating intervals. In Fig. 11A the

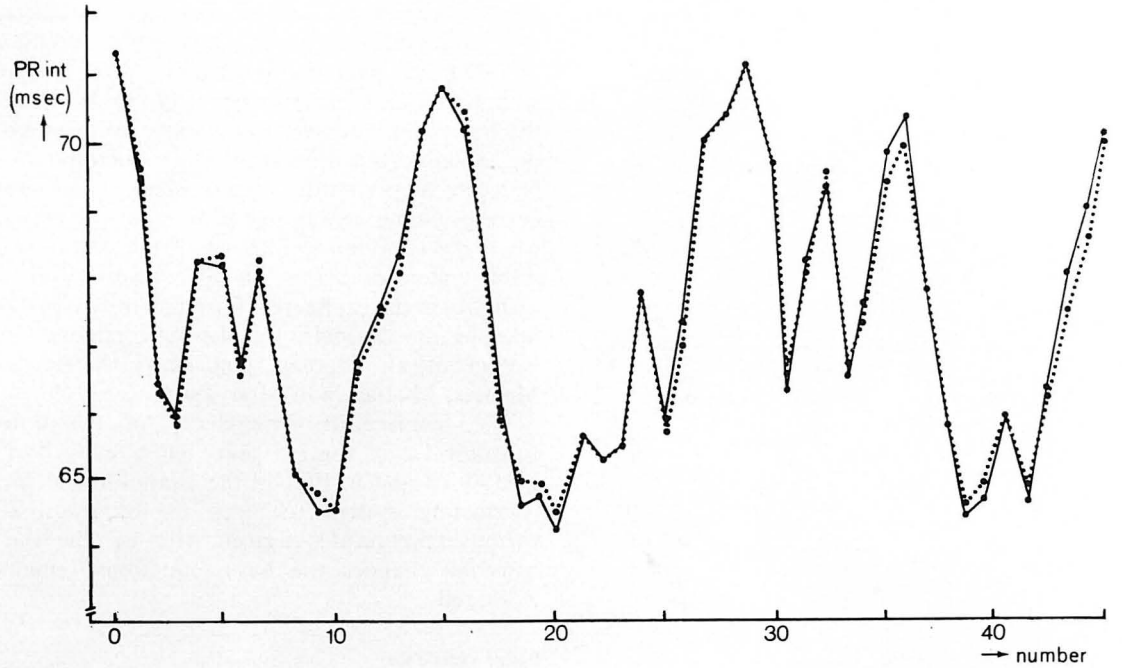

FIG. 8 *Representation of successive measured P–R intervals* (continuous line) *and the computation of the model* (dashed line) *during random stimulation of the rat heart* in vivo.

upper trace shows the activation of the right atrium of a rat heart, the lower trace the activation of the left atrium. The oscilloscope is triggered by the stimulation pulse. The stimulating bipolar electrodes are attached on the right atrial appendage. The stimulating interval is 280 msec. In Fig. 11B the stimulating interval is changed to 140 msec. The time between the intrinsic deflections of the atrial complexes changes less than 0·3 msec. The variations of the atrial conduction time during constant stimulation are also in the order of magnitude of 0·3 msec (see Fig. 11C, which shows again recordings as in Fig. 11A at a stimulating interval of 280 msec). From these measurements, also carried out with other stimulating intervals, we conclude that there are no striking changes ($>0{\cdot}3$ msec) in conduction over the atria as function of the stimulating interval. That means that the measured changes of delay between stimulating pulse and ventricular response are caused by the A-V node. Furthermore, it can be seen that the intervals between stimulus artefacts and intrinsic deflections of right and left atrial bipolar leads remains constant (within 0·3 msec) after changing back and forth the stimulus interval from 280 to 140 msec. It was therefore decided to use stimulus intervals for actual P–P intervals.

Discussion

With the theory developed above it is possible to calculate the A-V conduction time g of test atrial systoles initiated at various times τ after each sixteenth stimulating pulse with basic interval a. Using the formula for the step functions we get the result:

$$g = \rho(\tau) + g_{n,\infty}(a)e^{-\lambda\tau}$$

In Fig. 12 the A-V conduction times $g_{n,\infty}$ of the measured steady states are shown (squares). The open and filled circles indicate respectively the calculated and measured A-V conduction times of test atrial impulses initiated at varying intervals after each sixteenth basic stimulus at a cycle length of 220 msec. The open and filled

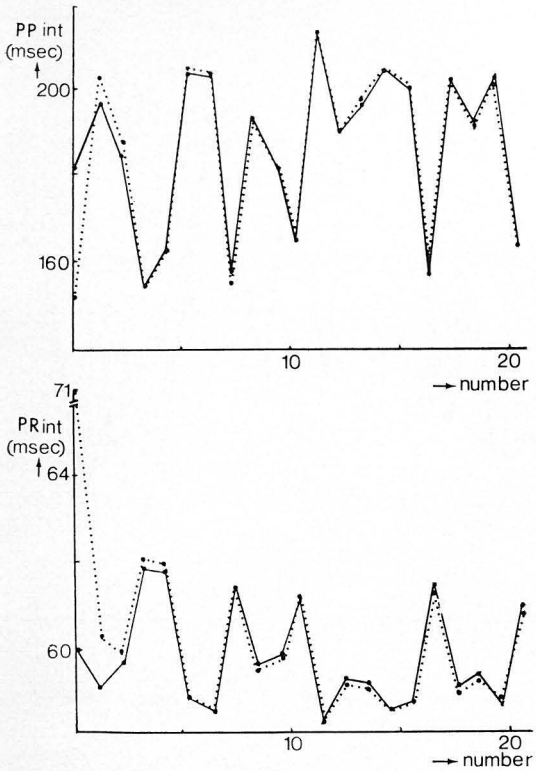

FIG. 9 *Plot of twenty successive measured P–P* (A) *and P–R* (B) *intervals* (continuous lines) *and the model computations* (dashed lines) *using measured R–R intervals.*

triangles represent resp. calculated and measured A-V conduction times for test atrial impulses initiated at various intervals after sixteen stimuli at a basic cycle length of 125 msec. When the heart is stimulated with a basic cycle length of 220 msec the difference of conduction time between a premature atrial systole and the corresponding steady state interval increases when the stimulating interval of the premature atrial systole decreases. So no recovery of conductivity in the rat heart is found, contrary to the findings of Merideth for the A-V conducting system of an exposed dog heart (Merideth, Mendez, Mueller, and Moe, 1968).

The temperature dependency of the time constant $1/\lambda$ of the rat heart has already been mentioned and in Fig. 13 the adaptation of the conducting system to steps in frequency at various temperatures is given. Although the time constant changes the basic equations remain unaltered.

Final remarks

In his editorial, Brody (1970) has outlined the controversial viewpoints about the origin of the irregular ventricular rhythm in patients with atrial fibrillation. In other studies (Bootsma *et al.*, 1970; Strackee, Hoelen, Zimmerman, and Meijler, 1971), it has been demonstrated that the A-V node cannot be solely responsible for the

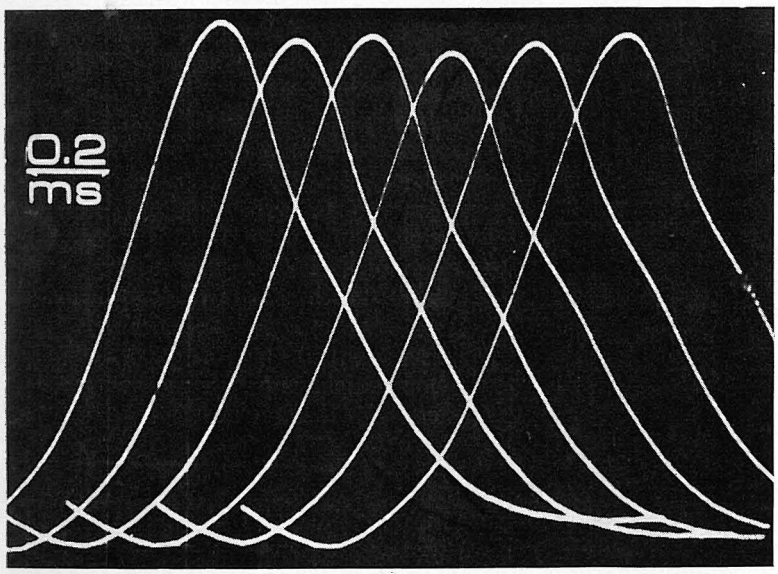

FIG. 10 *Electrical activity of the left ventricle at different stimulating intervals* τ ($\tau = 300$, *resp. 250, 200, 180, 160, and 140 msec*). (*The relative position of the complexes is arbitrary.*)

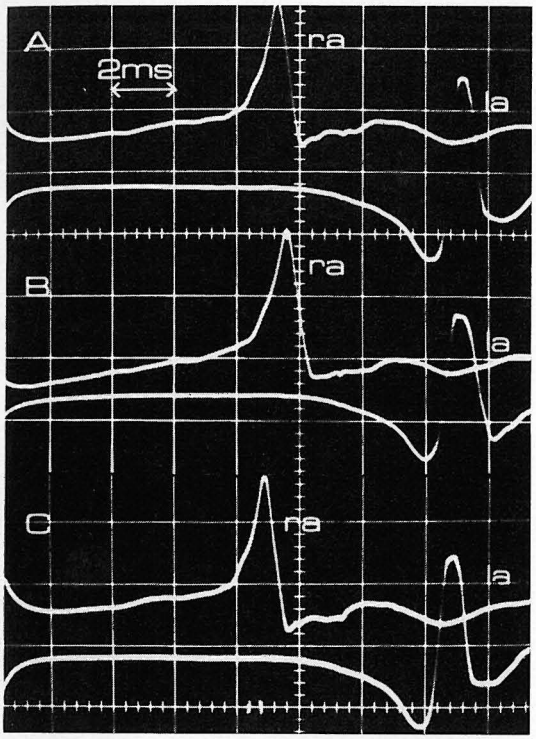

FIG. 11 *Electrograms of the right and left atrium during right atrial appendage stimulation (intervals:* A *280,* B *140, and* C *280 msec).*

irregular ventricular rhythm during atrial fibrillation. The model developed in this paper covers quantitatively A-V nodal conductive properties obtained without jeopardizing the A-V nodal tissue. In the experiments presented here all atrial activations were conducted to the ventricles. However, in atrial fibrillation many atrial activations are blocked in the A-V node. The model has therefore been extended to include conductive properties after blocking of atrial activations in the A-V node. The results of these experiments will be described in a subsequent paper. The model will also be used to study A-V nodal conduction in other mammals, especially man. At the same time, it is felt that the model can be used for pharmacological studies of the A-V node. For instance, the effect of digitalis on the A-V node can be ascertained quantitatively.

We gratefully acknowledge the help of Dr. Allen M. Scher (University of Washington, Seattle, Washington, U.S.A.) with the preparation of this paper and the participation in this research of Ineke E. Frederik, Jan M. Schoenmaker, and Ruud M. de Vos Burchart.

References

Bootsma, B. K., Hoelen, A. J., Strackee, J., and Meijler, F. L. (1970). Analysis of R–R intervals in patients with atrial fibrillation at rest and during exercise. *Circulation*, **41**, 783–794.

Brody, D. A. (1970). Ventricular rate patterns in atrial fibrillation. *Circulation*, **41**, 733–735.

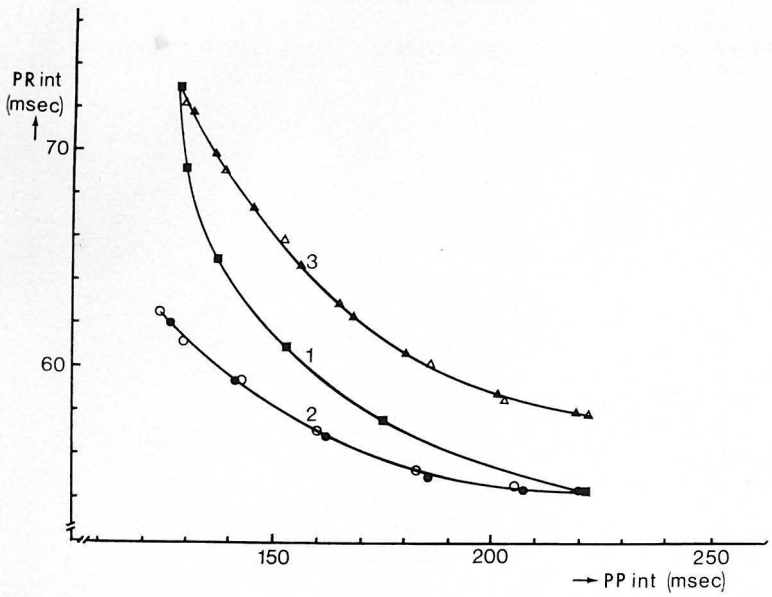

FIG. 12 1: *steady state relation between P–R and P–P intervals.* 2, 3: *computed* (○ *resp.* △) *and measured* (● *resp.* ▲) *P–R intervals of a premature beat after sixteen stimuli at a basic cycle length of 220 resp. 125 msec.*

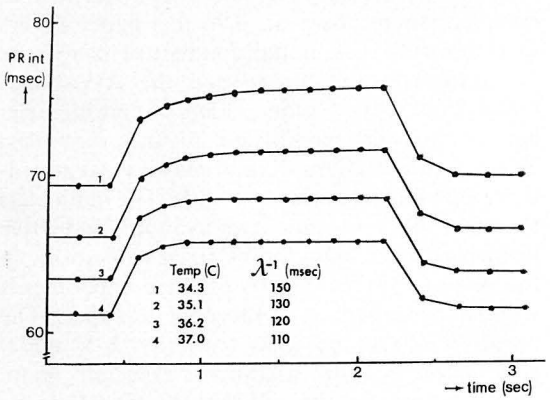

FIG. 13 *Course of P–R interval after changing back and forth the stimulating interval from 220 to 160 msec at different temperatures together with the time constants.*

Goovaerts, H. G., Schneider, H., and Zimmerman, A. N. E. (1971). An isolated current source supplied by a carrier for experimental stimulation of the heart. *Medical Research Engineering*, **10**, No. 4, 28–30.

Horan, L. G., and Kistler, J. C. (1961). Study of ventricular response in atrial fibrillation. *Circulation Research*, **9**, 305–311.

Meijler, F. L., Offerijns, F. G. J., Willebrands, A. F., and Groen, J. (1959). Contractiemechanisme en elektrolythuishouding van het geïsoleerde, overlevende rattehart, mede in verband met de werking van insuline. *Nederlands Tijdschrift voor Geneeskunde*, **103**, 1479–1486.

Merideth, J., Mendez, C., Mueller, W. J., and Moe, G. K. (1968). Electrical excitability of atrioventricular nodal cells. *Circulation Research*, **23**, 69–85.

Moe, G. K., and Abildskov, J. A. (1964). Observations on the ventricular dysrhythmia associated with atrial fibrillation in the dog heart. *Circulation Research*, **14**, 447–460.

Moore, E. N. (1967). Observations on concealed conduction in atrial fibrillation. *Circulation Research*, **21**, 201–208.

Strackee, J., Hoelen, A. J., Zimmerman, A. N. E., and Meijler, F. L. (1971). Artificial atrial fibrillation in the dog: an artefact? *Circulation Research*, **28**, 441–445.

Appendix

In general the n-th P–R interval is:

$$g_n = g_{n,\infty} + (g_{n-1} - g_{n,\infty})e^{-\lambda\tau_n} \qquad (7)$$

thus:

$$g_{n-1} = g_{n-1,\infty} + (g_{n-2} - g_{n-1,\infty})e^{-\lambda\tau_{n-1}} \qquad (8)$$

Substitution of (8) in (7) gives:

$$g_n = g_{n,\infty}(1-e^{-\lambda\tau_n}) + g_{n-1,\infty}(1-e^{-\lambda\tau_{n-1}})e^{-\lambda\tau_n} + g_{n-2}e^{-\lambda(\tau_n+\tau_{n-1})}$$

A further substitution of $g_{n-k}(k=2, 3, \ldots m)$, gives:

$$g_n = \rho(\tau_n) + \sum_{j=1}^{m} \rho(\tau_{n-j}) \exp\{-\lambda \sum_{i=o}^{j-1} \tau_{n-i}\} + g_{n-m-1} \cdot \prod_{j=o}^{m} e^{-\lambda\tau_{n-j}}$$

where $\rho(\tau_n) = g_{n,\infty}(1-e^{-\lambda\tau_n})$

As $e^{-\lambda\tau_n} < 0{\cdot}3$, $\prod_{j=o}^{k} e^{-\lambda\tau_{n-j}} < 0{\cdot}3^{k+1}$

This implies that terms with $k \geqslant 4$ can be omitted because they are less than 0·3 msec, the error in the experimental results.

Thus a P–R interval at a given moment can be described as a function of only the five directly preceding P–P intervals:

$$g_n = \rho(\tau_n) + \sum_{j=1}^{m=4} \rho(\tau_{n-j}) \exp\{-\lambda \sum_{i=o}^{j-1} \tau_{n-i}\}$$